Nonlinear Dyn (2022) 107:3669–3682
https://doi.org/10.1007/s11071-021-07153-0

ORIGINAL PAPER

Exploiting expansion basis sparsity for efficient stochastic response determination of nonlinear systems via the Wiener path integral technique

Yuanjin Zhang · Ioannis A. Kougioumtzoglou · Fan Kong

Received: 25 September 2021 / Accepted: 14 December 2021 / Published online: 26 January 2022

Abstract The computational efficiency of the Wiener path integral (WPI) technique for determining the stochastic response of diverse nonlinear dynamical systems is enhanced herein by relying on advanced compressive sampling concepts and tools. Specifically, exploiting the sparsity of appropriately selected expansions for the joint response probability density function (PDF), and leveraging the localization capabilities of the WPI technique for direct evaluation of specific PDF points, yield an underdetermined linear system of equations to be solved for the PDF expansion coefficients. This is done by resorting to L_p-norm ($0 < p < 1$) minimization formulations and algorithms, which exhibit an enhanced sparsity-promoting behavior compared to standard L_1-norm minimization approaches. This translates into a significant reduction of the associated computational cost. In fact, for approximately the same accuracy degree, it is shown that the herein developed technique based on L_p-norm ($0 < p < 1$) minimization requires, in some cases, even up to 40% fewer boundary value problems to be solved as part of the solution scheme than a standard L_1-norm minimization approach. The reliability of the technique is demonstrated by comparing WPI-based response PDF estimates with pertinent Monte Carlo simulation (MCS) data (10,000 realizations). In this regard, realizations compatible with the excitation stochastic process are generated, and response time-histories are obtained by integrating numerically the nonlinear system equations of motion. Next, MCS-based PDF estimates are computed based on statistical analysis of the response time-histories. Several numerical examples are considered pertaining to various stochastically excited oscillators exhibiting diverse nonlinear behaviors. These include a Duffing oscillator, an oscillator with asymmetric nonlinearities, and a nonlinear vibro-impact oscillator.

Keywords Sparse representations · Compressive sampling · Nonlinear systems · Stochastic dynamics · Path integral

Y. Zhang
School of Safety Science and Emergency Management, Wuhan University of Technology, 122 Luoshi Road, Wuhan, Hubei 430070, China
e-mail: ylzhyj@whut.edu.cn

I. A. Kougioumtzoglou (✉)
Department of Civil Engineering and Engineering Mechanics, Columbia University, 500 West 120th Street, New York 10027, NY, USA
e-mail: ikougioum@columbia.edu

F. Kong
School of Civil Engineering and Architecture, Wuhan University of Technology, 122 Luoshi Road, Wuhan, Hubei 430070, China
e-mail: kongfan@whut.edu.cn

1 Introduction

Ever-increasing computational power, novel signal processing techniques, advanced experimental setups, and progress in emerging and transformative technologies have contributed to a highly complex mathemat-

ical modeling of the governing equations of diverse dynamical systems; see, for instance, indicative examples from nano-mechanics [1] and energy harvesting [2]. In fact, developing versatile techniques for determining system response and reliability statistics, accurately and in a computationally efficient manner, has been a persistent challenge in the field of stochastic engineering dynamics; see, indicatively, [3–5] for a broad perspective on the capabilities and limitations of various solution techniques developed over the past six decades.

One of the promising techniques developed recently by Kougioumtzoglou and co-workers relies on the concept of Wiener path integral (WPI), which relates to the generalization of integral calculus to functionals (e.g., [6–8]). The WPI technique is capable of determining the joint response transition probability density function (PDF) of multi-degree-of-freedom (MDOF) systems exhibiting a wide range of nonlinear/hysteretic behaviors [9,10]. Further, it can account for diverse non-white and non-Gaussian stochastic process modeling [11], while its accuracy has been enhanced recently based on a quadratic approximation of the WPI functional series expansion [12]. Furthermore, high-dimensional systems can be readily addressed by relying on a variational formulation with mixed fixed/free boundary conditions, which renders the computational cost independent of the total number of stochastic dimensions [13]. Moreover, it was shown in [14] that the computational cost can be reduced drastically by employing sparse representations for the system response PDF in conjunction with compressive sampling schemes and group sparsity concepts. Also, the efficacy of employing global multi-dimensional bases for determining the non-stationary joint response PDF in a direct manner was demonstrated in [15].

In this paper, the computational efficiency of the WPI technique is enhanced by relying on advanced compressive sampling concepts and tools; see also [16] for a recent review paper. This is done by employing sparse expansions for the system response PDF and by relying on the localization capabilities of the WPI technique for direct evaluation of specific PDF points. This yields an underdetermined linear system of algebraic equations to be solved via L_p-norm ($0 < p < 1$) minimization algorithms for obtaining the PDF expansion coefficient vector. In comparison with the L_1-norm minimization approach proposed in [14], the L_p-norm ($0 < p < 1$) minimization formulation developed herein exhibits an enhanced sparsity-promoting behavior. This translates into fewer PDF points to be obtained by the WPI for formulating the underdetermined system of equations. In other words, the same degree of accuracy is attained in estimating the system response PDF at a reduced computational cost. The reliability of the technique is demonstrated by comparing WPI-based results with pertinent Monte Carlo simulation (MCS) data. This is done in conjunction with various stochastically excited oscillators exhibiting diverse nonlinear behaviors. These include a Duffing oscillator, an oscillator with asymmetric nonlinearities, and a nonlinear vibro-impact oscillator.

2 Mathematical formulation

2.1 Wiener path integral technique: selected aspects

In this section, fundamental concepts and basic aspects of the WPI technique are reviewed for completeness, in conjunction with a stochastically excited single-degree-of-freedom (SDOF) nonlinear oscillator for notation simplicity and tutorial effectiveness. The interested reader is also directed to [13] for a recent extension of the technique to address high-dimensional nonlinear systems, as well as to [11] for a generalization to account for non-white and non-Gaussian stochastic excitation.

Specifically, consider the governing equation of motion

$$\ddot{x} + c\dot{x} + kx + g(x, \dot{x}) = w(t) \tag{1}$$

where x is the nonlinear system response, and a dot over a variable denotes differentiation with respect to time t; c, k are the damping and stiffness coefficients, respectively; and $g(x, \dot{x})$ is an arbitrary nonlinear function. The excitation $w(t)$ represents a Gaussian zero-mean white noise process with a constant power spectrum value equal to S_0.

Next, following [11] (see also [8] for a broader perspective), the joint transition PDF $p(x_f, \dot{x}_f, t_f | x_i, \dot{x}_i, t_i)$ of the oscillator response from the initial state $(x_i, \dot{x}_i, t_i)$ to the final state $(x_f, \dot{x}_f, t_f)$ can be expressed as a functional integral over the space of all possible paths $C\{x_f, \dot{x}_f, t_f; x_i, \dot{x}_i, t_i\}$ in the form

$$p(x_f,\dot{x}_f,t_f|x_i,\dot{x}_i,t_i) = \int_{\{x_i,\dot{x}_i,t_i\}}^{\{x_f,\dot{x}_f,t_f\}} \exp\left(-\int_{t_i}^{t_f} L(x,\dot{x},\ddot{x})dt\right)[dx(t)] \tag{2}$$

where $dx(t)$ denotes a functional measure, and $L(x,\dot{x},\ddot{x})$ represents the Lagrangian functional given by

$$L(x,\dot{x},\ddot{x}) = \frac{[\ddot{x}+c\dot{x}+kx+g(x,\dot{x})]^2}{4\pi S_0} \tag{3}$$

Further, according to calculus of variations [17] (see also Appendix for more details), the functional integral of Eq. (2) can be approximately evaluated by considering only the "most probable path" x_c, which satisfies the condition

$$\delta\int_{t_i}^{t_f} L(x_c,\dot{x}_c,\ddot{x}_c)dt = 0 \tag{4}$$

In this regard, Eq. (4) yields the Euler–Lagrange equation

$$\frac{\partial L}{\partial x_c} - \frac{\partial}{\partial t}\frac{\partial L}{\partial \dot{x}_c} + \frac{\partial^2}{\partial t^2}\frac{\partial L}{\partial \ddot{x}_c} = 0 \tag{5}$$

in conjunction with the boundary conditions

$$\begin{aligned} x_c(t_i) &= x_i, & \dot{x}_c(t_i) &= \dot{x}_i,\\ x_c(t_f) &= x_f, & \dot{x}_c(t_f) &= \dot{x}_f \end{aligned} \tag{6}$$

Solving Eqs. (5)–(6) for x_c and substituting into Eq. (2) yield an approximate closed-form expression for the transition PDF in the form

$$p(x_f,\dot{x}_f,t_f|x_i,\dot{x}_i,t_i) \approx C\exp\left(-\int_{t_i}^{t_f} L(x_c,\dot{x}_c,\ddot{x}_c)dt\right) \tag{7}$$

where C is a normalization constant determined by

$$\int_{-\infty}^{+\infty}\int_{-\infty}^{+\infty} p(x_f,\dot{x}_f,t_f|x_i,\dot{x}_i,t_i)dx_f d\dot{x}_f = 1 \tag{8}$$

It is noted that the most probable path approximation has exhibited a relatively high degree of accuracy in various diverse applications [10,11,13–15]. In fact, as proved in [18], for the case of linear systems the most probable path approximation yields the exact joint response PDF. The interested reader is also directed to [12] for a recent enhancement of the accuracy degree of the technique based on a quadratic approximation, which accounts for fluctuations around the most probable path as well.

2.2 Joint response PDF determination based on sparse expansions and L_p-norm ($0 < p < 1$) minimization

It can be readily seen that a brute-force numerical implementation of the WPI technique requires the discretization of the effective PDF domain into N points in each dimension, followed by the solution of a boundary value problem (BVP) described by Eqs. (5)–(6) corresponding to each and every point. Clearly, the computational cost increases exponentially with increasing number of dimensions; see also [13] for a relevant discussion. Thus, alternative more efficient formulations have been developed recently by relying on appropriate PDF expansions [15,19]. In this regard, the problem of evaluating the joint response PDF is recast into determining the PDF expansion coefficient vector. This yields a significantly reduced number of BVPs of the form of Eq. (5) to be solved, ordinarily equal to the number of the PDF expansion coefficients. As shown in [14], the required number of BVPs can be further reduced by resorting to compressive sampling concepts and tools (e.g., [16,20,21]) for formulating an underdetermined system of algebraic equations to be solved for the sparse PDF expansion coefficient vector.

In this section, the computational efficiency of the WPI technique is enhanced by relying on L_p-norm ($0 < p < 1$) minimization algorithms for formulating and solving the underdetermined algebraic system of equations for the PDF expansion coefficients. This development can be construed as an extension and generalization of [14], where the response PDF coefficient vector was determined based on a rather standard L_1-norm minimization formulation. Specifically, a solution approach based on L_p-norm ($0 < p < 1$) exhibits an enhanced sparsity-promoting behavior compared to L_1-norm [16], and thus, fewer BVPs need to be solved for obtaining PDF points to be used in the underdetermined system of equations for the expansion coefficients. In fact, as shown in the numerical examples in Sect. 3, the L_p-norm ($0 < p < 1$) approach exhibits a higher degree of accuracy in estimating the system response PDF at a reduced computational cost.

In the ensuing analysis, considering fixed initial conditions at $t_i = 0$, the non-stationary joint response PDF corresponding to the nonlinear oscillator of Eq. (1) is expressed in the form

$$p(x, \dot{x}, t) \approx \exp(\mu(x, \dot{x}, t)) \tag{9}$$

or, alternatively,

$$p(x, \dot{x}, t) \approx \nu(x, \dot{x}, t) \tag{10}$$

where $\mu(x, \dot{x}, t)$ and $\nu(x, \dot{x}, t)$ are approximating expansions with appropriately selected bases. Indicative candidates include multivariate polynomials [22], wavelets [23], and positive definite functions [24]. Without loss of generality and based on the findings in [15], two distinct approximating approaches are employed in the following in conjunction with Eq. (9) or Eq. (10).

First, the multivariate polynomial and the wavelet bases are used for the spatial and the temporal dimensions, respectively, whereas a Kronecker-type expansion (e.g., [25]) of $\mu(x, \dot{x}, t)$ in Eq. (9) is considered in the form

$$\boldsymbol{\mu} = (\mathbf{P} \otimes \mathbf{D}_t)\mathbf{c} \tag{11}$$

In Eq. (11), $\otimes$ denotes the Kronecker operator; $\mathbf{D}_t \in \mathbb{R}^{N_t \times N_t}$ represents an one-dimensional harmonic wavelet basis [26] corresponding to the time domain; $\mathbf{P} \in \mathbb{R}^{N_p \times N_p}$ is the monomial basis referring to the spatial domain $(x, \dot{x})$; $\boldsymbol{\mu} \in \mathbb{R}^{N_t N_p \times 1}$ represents the measurements $\mu(x, \dot{x}\,, t) = ln(p(x, \dot{x}, t))$ obtained by the WPI technique as described in Sect. 2.1; $\mathbf{c} \in \mathbb{R}^{n \times 1}$ denotes the coefficient vector to be determined. In this regard, $n = N_t N_p$ measurements are required by the WPI to determine the non-stationary joint response PDF of the nonlinear system, where N_t and N_p pertain to a discretization of the time and the space domains, respectively. Note, in passing, that a multivariate polynomial expansion is a reasonable choice for a wide range of nonlinear systems. The rationale relates to the fact that in many cases the nonlinear response PDF can be viewed as a perturbation (not necessarily small) from the corresponding linear system PDF. In fact, the linear oscillator response PDF is Gaussian, with an exponent represented exactly by a 2^{nd}-order polynomial expansion. Thus, it is anticipated that the response PDF of various nonlinear oscillators can be captured efficiently by employing a higher-order polynomial expansion, where only few of the higher-order monomials are active. In other words, a polynomial basis for $\mathbf{P}$ is expected to exhibit sparsity. This attribute has been exploited already in [14] by utilizing an L_1-norm minimization formulation for determining the PDF expansion coefficients.

Nevertheless, various oscillators exhibit non-smooth nonlinear behaviors, which cannot be captured efficiently by polynomial approximations. In such cases, a polynomial basis is not sparse and alternative approximations need to be explored. In this regard, the strategy of approximating ν in Eq. (10) by utilizing a wavelet basis both for the spatial and the temporal dimensions, in conjunction with a Kronecker expansion, is considered in the ensuing analysis; that is, Eq. (10) takes the form

$$\boldsymbol{\nu} = (\mathbf{D}_{s1} \otimes \mathbf{D}_{s2} \otimes \mathbf{D}_t)\mathbf{c} \tag{12}$$

where $\mathbf{D}_{s1} \in \mathbb{R}^{N_{s1} \times N_{s1}}$ and $\mathbf{D}_{s2} \in \mathbb{R}^{N_{s2} \times N_{s2}}$ represent one-dimensional harmonic wavelet bases corresponding to the spatial domain; and $\boldsymbol{\nu} \in \mathbb{R}^{N_t N_p \times 1}$ represent the measurements $\nu(x, \dot{x}, t) = p(x, \dot{x}, t)$ obtained by the WPI technique as described in Sect. 2.1. In this case, $n = N_{s1} N_{s2} N_t$ measurements are required by the WPI, where N_{s1} and N_{s2} pertain to a discretization of the 2-dimensional spatial domain.

Next, a solution approach based on L_p-norm ($0 < p < 1$) minimization is developed for determining the response PDF expansion coefficients. In passing, note that approaches based on L_p-norm have exhibited superior sparsity-promoting behaviors compared to L_1-norm in a variety of engineering dynamics applications, such as spectral analysis and estimation under limited data [27]; see also [16] for a broad perspective.

Specifically, for a given time instant $t = t_j$ ($j = 1, ..., N_t$) and using $r < n_j$ PDF measurements, where $n_j = N_p$ and $n_j = N_{s1} N_{s2}$ referring to Eqs. (11) and (12), respectively, Eqs. (11) and (12) are cast into an underdetermined linear system of equations of the form

$$\boldsymbol{y}_{0,j} = \boldsymbol{\Phi} \boldsymbol{y}_j = \mathbf{A}\mathbf{c}_j \tag{13}$$

where

$$\boldsymbol{y}_j = \begin{cases} \boldsymbol{\mu}_j & \text{referring to Eq. (11)} \\ \boldsymbol{v}_j & \text{referring to Eq. (12)} \end{cases} \tag{14}$$

and

$$\mathbf{A} = \begin{cases} \boldsymbol{\Phi}\mathbf{P} & \text{referring to Eq. (11)} \\ \boldsymbol{\Phi}(\mathbf{D}_{s1} \otimes \mathbf{D}_{s2}) & \text{referring to Eq. (12)} \end{cases} \tag{15}$$

In Eqs. (13)–(15), $\boldsymbol{\mu}_j$ and $\boldsymbol{v}_j$ are the $n_j \times 1$ measurement vectors corresponding to time instant $t = t_j$; $\boldsymbol{\Phi}$ is an $r \times n_j$ matrix , which deletes randomly rows from y_j and the expansion basis; and $\mathbf{c}_j$ is the $n_j \times 1$ coefficient vector to be determined corresponding to $t = t_j$.

Further, an L_p-norm $(0 < p < 1)$ minimization formulation is proposed for solving Eq. (13). This takes the form

$$\min |\mathbf{c}_j|_{L_p}, \quad \text{subject to} \quad \boldsymbol{y}_{0,j} = \mathbf{A}\mathbf{c}_j \tag{16}$$

In the following, the $p = 1/2$ norm is used since, as discussed in [27,28], the sparsest solution is obtained for $1/2 \leq p < 1$, whereas the sparsity degree remains relatively unaffected for $0 < p < 1/2$. Next, to minimize Eq. (16), the Lagrangian $L(c_j, \lambda)$ is introduced as:

$$L(\mathbf{c}_j, \lambda) = \sum_{n_j} |c_{j,i}|^{\frac{1}{2}} + \lambda^T(\mathbf{A}\mathbf{c}_j - \boldsymbol{y}_{0,j}) \tag{17}$$

The partial derivatives of Eq. (17) with respect to $\mathbf{c}_j$ and λ become zero for:

$$\mathbf{c}_j = \mathbf{Q}\mathbf{A}'(\mathbf{A}\mathbf{Q}\mathbf{A}')^{-1}\boldsymbol{y}_{0,j} \tag{18}$$

where

$$\mathbf{Q} = \text{diag}(|\mathbf{c}_j|^{\frac{3}{2}}) \tag{19}$$

Equation (18) can be solved in an iterative manner, i.e., the k^{th} iteration yields

$$\mathbf{c}_{j,k} = \mathbf{Q}_{k-1}\mathbf{A}'(\mathbf{A}\mathbf{Q}_{k-1}\mathbf{A}')^{-1}\boldsymbol{y}_{0,j} \tag{20}$$

where

$$\mathbf{Q}_{k-1} = \text{diag}(|\mathbf{c}_{j,k-1}|^{\frac{3}{2}}) \tag{21}$$

Note that this algorithm is equivalent to a weighted L_2-norm minimization [29], i.e.,

$$\min \sum \omega_i c_{j,i}^2, \quad \text{subject to} \quad \boldsymbol{y}_{0,j} = \mathbf{A}\mathbf{c}_j \tag{22}$$

where $\omega_i = |c_{j,i,k-1}|^{-3/2}$. Since the solution is sparse, the values of many $c_{j,i}$ will tend toward zero. To avoid division by zero in ω_i as the algorithm converges to a solution, a decreasing parameter ϵ is introduced to regularize the optimization problem [30]. This yields

$$\mathbf{Q}_{k-1} = \text{diag}(((|\mathbf{c}_{j,k-1}| + \sqrt{\epsilon_j} \cdot \text{mean}(|\mathbf{c}_{j,k-1}|))^2)^{\frac{3}{4}}) \tag{23}$$

with

$$\epsilon_j = \frac{\epsilon_{j-1}}{10} \tag{24}$$

where an indicative starting value for ϵ_j is $\epsilon_0 = 0.01$. For each ϵ_j, Eq. (20) is repeated until satisfying the condition

$$\frac{\|\mathbf{c}_{j,k} - \mathbf{c}_{j,k-1}\|_2}{\|\mathbf{c}_{j,k-1}\|_2} < \frac{\sqrt{\epsilon_j}}{100} \tag{25}$$

It is remarked that the generalization of the developed technique to treat MDOF nonlinear systems is rather straightforward. Specifically, for an m-DOF system, the expansion in Eq. (9), or alternatively in Eq. (10), corresponds to the system $2m$-variate joint response PDF. This yields Eq. (13) to be solved for the expansion coefficient vector based on L_p-norm $(0 < p < 1)$ minimization. Note that in this case the dimensions of the measurement vector $\boldsymbol{y}_{0,j}$ and the basis matrix $\mathbf{A}$ are appropriately augmented to account for the increase in the number of DOFs of the system.

2.3 Mechanization of the technique

The mechanization of the developed stochastic response determination technique based on L_p-norm $(0 < p < 1)$ minimization comprises the following steps:

(a) Construct the multivariate polynomial basis $\mathbf{P}$ for the spatial domain and the harmonic wavelet basis $\mathbf{D}_t$ for the temporal dimension in Eq. (11) (or, alternatively, the harmonic wavelet bases $\mathbf{D}_{s1}$, $\mathbf{D}_{s2}$, and $\mathbf{D}_t$ in Eq. (12)).

(b) For a specific $t = t_j$, select r points in the spatial domain either randomly, or by utilizing certain optimality criteria (e.g., [31]).
(c) Determine the PDF measurement points $\boldsymbol{y}_{0,j}$ in Eq. (13) by solving Eqs. (5)–(6) and utilizing Eq. (7).
(d) Solve Eq. (16) for obtaining the sparse coefficient vector $\mathbf{c}_j$.
(e) Repeat steps (b-d) for $j = 1, .., N_t$ time instants and substitute $\mathbf{c}$ into Eq. (11) (or, alternatively, Eq. (12)) for determining the non-stationary system response PDF.

In passing, note that alternative to Kronecker product formulations, such as mesh-free approximation schemes based on positive definite functions, can be also employed for approximating the system response PDF and for deriving an underdetermined linear system of algebraic equations in the form of Eq. (13); see also [15] for a relevant discussion.

3 Numerical examples

In this section, three distinct numerical examples pertaining to oscillators with diverse nonlinear behaviors are considered for assessing the reliability of the developed technique. In this regard, the response PDF determined by $L_{1/2}$-norm minimization is compared with estimates based on L_1-norm minimization and on MCS (10,000 realizations). Clearly, the degree of computational efficiency enhancement obtained by $L_{1/2}$-norm minimization depends on a variety of factors, such as the nonlinearity type and the selected expansion basis. Nevertheless, for approximately the same accuracy degree, it is shown that the herein developed technique requires, in some cases, even up to 40% fewer PDF points to be obtained by the WPI than a standard L_1-norm minimization approach.

3.1 Duffing nonlinear oscillator

Consider a Duffing nonlinear oscillator subject to Gaussian white noise, whose dynamics is governed by Eq. (1) with

$$g(x, \dot{x}) = \varepsilon k x^3 \tag{26}$$

and $\varepsilon > 0$ denotes a parameter accounting for the nonlinearity degree. The oscillator is considered to be initially at rest, whereas an eighth-order polynomial expansion is used for the basis $\mathbf{P}$ in Eq. (11). This translates into $n_j = N_p = 45$ coefficients to be determined for a specific time instant. Also, the harmonic wavelet basis $\mathbf{D}_t$ in Eq. (11) has $N_t = 16$ elements. In the following, the parameter values used are $S_0 = 0.1911, k = 0.3, c = 1, \varepsilon = \frac{5}{3}$. Note that the exact analytical expression of the stationary joint response PDF corresponding to the Duffing oscillator of Eq. (26) is available and given by (e.g., [32])

$$p(x, \dot{x}) = C \exp\left[\frac{-c}{\pi S_0}\left(\frac{kx^2}{2} + \frac{\varepsilon x^4}{4} + \frac{\dot{x}^2}{2}\right)\right] \tag{27}$$

where C is a normalization constant.

Next, Fig. 1 shows the determined polynomial expansion coefficients for $t = 1.2s$ using both $r/n_j = 0.6$ and $r/n_j = 0.7$. It is seen that both the $L_{1/2}$-norm and the L_1-norm approaches exhibit high accuracy in recovering the sparse coefficient vector for $r/n_j = 0.7$ as compared to estimates based on $r/n_j = 1$. However, the $L_{1/2}$-norm approach appears to yield a sparser (and more accurate) solution when fewer PDF measurements are used, i.e., for $r/n_j = 0.6$. This is further corroborated in Fig. 2, where the response displacement and velocity PDFs are plotted corresponding to $t = 1.2s$. Comparisons between PDF estimates obtained by the $L_{1/2}$-norm and the L_1-norm approaches for $r/n_j = 0.6$, and by MCS data (10,000 realizations), demonstrate an enhanced accuracy degree exhibited by the $L_{1/2}$-norm over the L_1-norm. Results based on a brute-force implementation of the WPI technique relying on a discretization of the PDF effective domain are included as well.

Moreover, attention is directed to $t = 10s$ corresponding to the stationary phase of the response process. In fact, the exact stationary response PDF is given by Eq. (27) exhibiting a polynomial representation with only three active coefficients. In Fig. 3, the exact coefficient vector pertaining to Eq. (27) is compared with the coefficient vectors obtained by $L_{1/2}$-norm and by L_1-norm, both for $r/n_j = 0.45$ and for $r/n_j = 0.7$. It is seen that even when very few measurements are used, i.e., $r/n_j = 0.45$, $L_{1/2}$-norm is capable of successfully determining the expansion coefficients, demonstrating superior accuracy compared to L_1-norm. Note that approximately the same degree of accuracy is achieved by L_1 and $L_{1/2}$-norms for $r/n_j = 0.7$ at the expense, however, of additional computational cost related to the

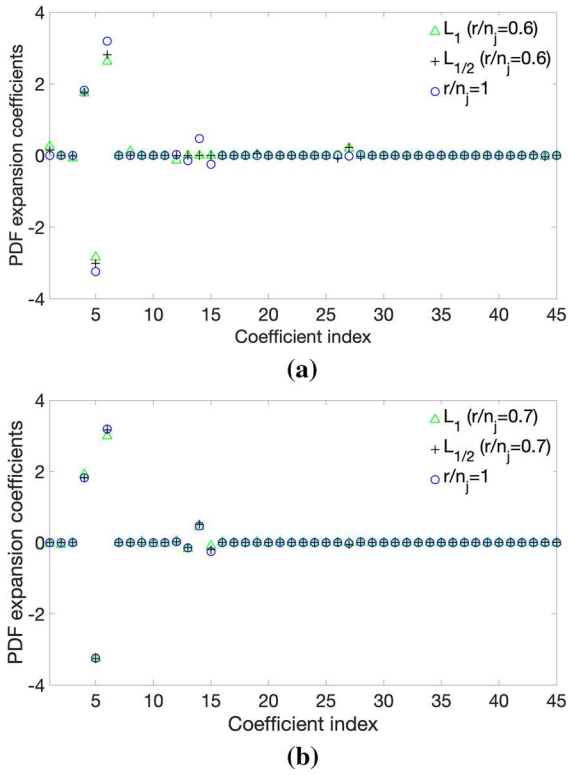

Fig. 1 Joint response PDF polynomial expansion coefficients corresponding to a Duffing nonlinear oscillator at $t = 1.2s$ with **a** $r/n_j = 0.6$ and **b** $r/n_j = 0.7$

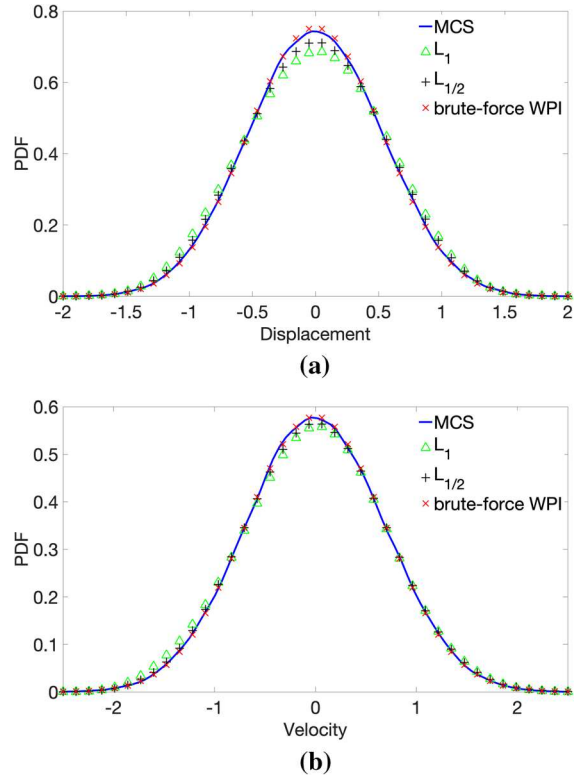

Fig. 2 Duffing nonlinear oscillator marginal response PDF at $t = 1.2s$: **a** displacement and **b** velocity; comparisons between $L_{1/2}$-norm and L_1-norm approaches for $r/n_j = 0.6$ and MCS data (10,000 realizations). Results based on a brute-force implementation of the WPI technique are included as well

increased number of BVPs to be solved. In other words, the enhanced sparsity-promoting capabilities of $L_{1/2}$-norm compared to L_1-norm yield accurate coefficient vector estimates by requiring fewer PDF measurement points, i.e., at a reduced computational cost. This is also supported by corresponding PDF estimates shown in Fig. 4 for $r/n_j = 0.45$, where comparisons with pertinent MCS data (10,000 realizations) demonstrate a higher degree of accuracy exhibited by the $L_{1/2}$-norm over the L_1-norm.

3.2 Oscillator with asymmetric nonlinearities

An oscillator with asymmetric nonlinearities is considered in this section to further assess the performance of the $L_{1/2}$-norm minimization formulation in conjunction with expansion bases exhibiting a moderate degree of sparsity. Specifically, compared to the Duffing oscillator in Sect. 3.1, more terms in the polynomial expansion are anticipated to be active due to the oscillator asymmetric nonlinear behavior, thus yielding a less sparse coefficient vector.

In this regard, the governing equation of motion is given by Eq. (1) with:

$$g(x, \dot{x}) = \epsilon k x^2 \tag{28}$$

where ϵ denotes a parameter accounting for the nonlinearity degree. The Kronecker expansion with an eighth-order polynomial basis is used, which leads to $n_j = N_p = 45$ coefficients to be determined for a specific time instant, whereas the harmonic wavelet basis $\mathbf{D}_t$ in Eq. (11) comprises $N_t = 16$ elements. In the following, the parameters $S_0 = 0.0637, k = 1, c = 0.2, \epsilon = 0.5$ are used.

Next, Fig. 5 shows the computed polynomial expansion coefficients for $t = 1s$ using both $r/n_j = 0.3$ and $r/n_j = 0.4$. Clearly, compared to $r/n_j = 1$, the $L_{1/2}$-norm approach exhibits a higher degree of accuracy

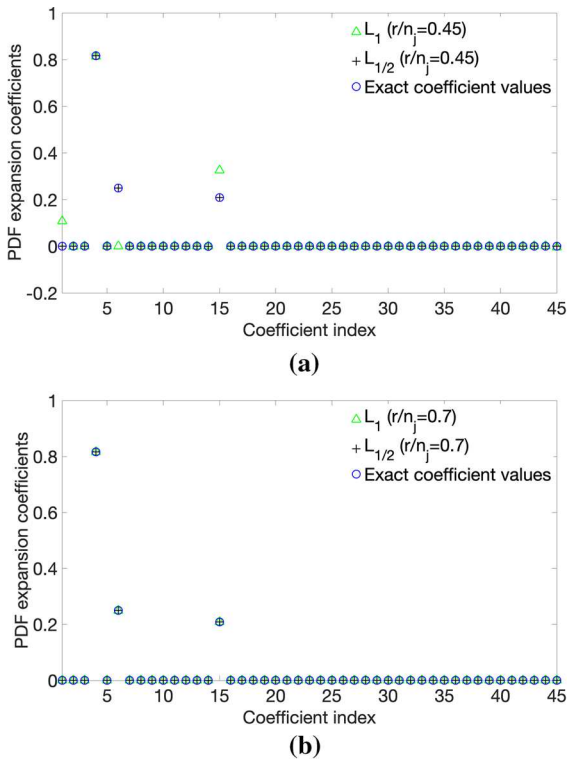

Fig. 3 Joint response PDF polynomial expansion coefficients corresponding to a Duffing nonlinear oscillator at $t = 10s$ (stationary phase) with **a** $r/n_j = 0.45$ and **b** $r/n_j = 0.7$; comparisons with the exact coefficient vector corresponding to Eq. (27)

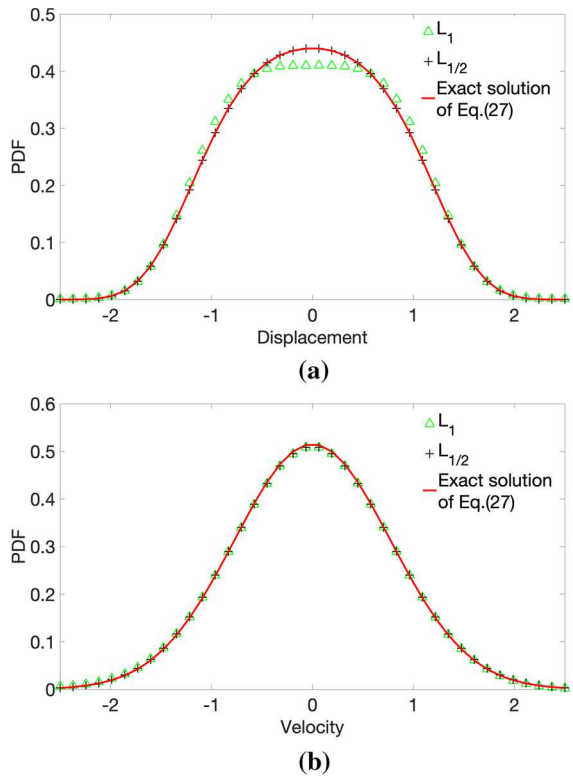

Fig. 4 Duffing nonlinear oscillator marginal response PDF at $t = 10s$ (stationary phase): **a** displacement and **b** velocity; comparisons between $L_{1/2}$-norm and L_1-norm approaches for $r/n_j = 0.45$, and the exact solution of Eq. (27)

over L_1-norm, especially when the number of available measurements r/n_j decreases. This is readily seen in Fig. 6, where the response displacement and velocity PDFs are plotted corresponding to $t = 1s$. Comparisons between PDF estimates obtained by the $L_{1/2}$-norm and the L_1-norm approaches for $r/n_j = 0.3$, and by MCS data (10,000 realizations) demonstrate superior accuracy exhibited by the $L_{1/2}$-norm over the L_1-norm. Results based on a brute-force implementation of the WPI technique relying on a discretization of the PDF effective domain are included as well.

Next, the time instant $t = 2s$ is considered for which the asymmetry in the response PDF is more prevalent than at $t = 1s$. In fact, as also seen in Fig. 7 where the corresponding coefficient vector is estimated both for $r/n_j = 0.7$ and for $r/n_j = 0.8$, more polynomial basis coefficients are active (compared to $t = 1s$) for capturing the asymmetric shape of the response PDF shown in Fig. 8, estimated for $r/n_j = 0.7$ by L_1-norm and by $L_{1/2}$-norm. Pertinent MCS-based estimates (10,000 realizations) are included as well. Obviously, even for this case where the target coefficient vector is less sparse than the one corresponding to the Duffing oscillator in Sect. 3.1, the $L_{1/2}$-norm approach exhibits superior accuracy over L_1-norm, especially for decreasing values of r/n_j. In other words, the same accuracy degree can be achieved with fewer measurement points, i.e., at a lower computational cost.

3.3 Nonlinear vibro-impact oscillator

In this section, a nonlinear vibro-impact oscillator is considered, whose governing equation is given by Eq. (1) with

$$g(x, \dot{x}) = \eta h(x) \tag{29}$$

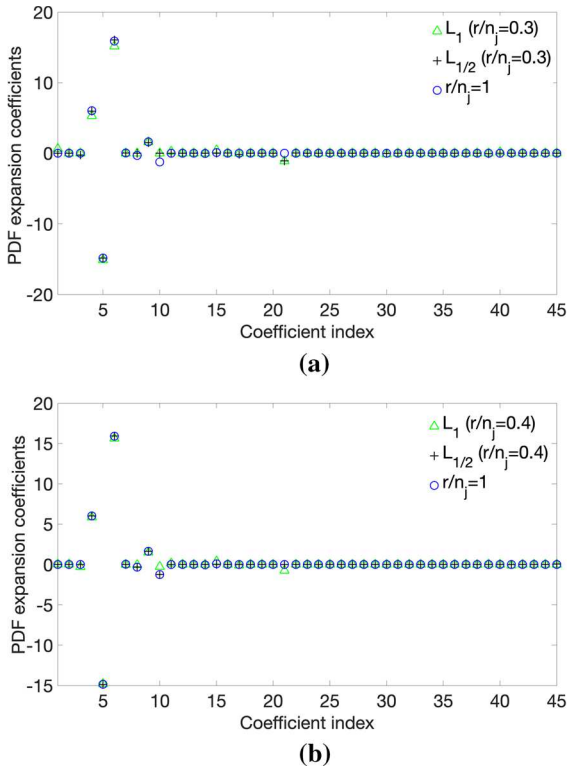

Fig. 5 Joint response PDF polynomial expansion coefficients corresponding to an oscillator with asymmetric nonlinearities at $t = 1s$ with **a** $r/n_j = 0.3$ and **b** $r/n_j = 0.4$

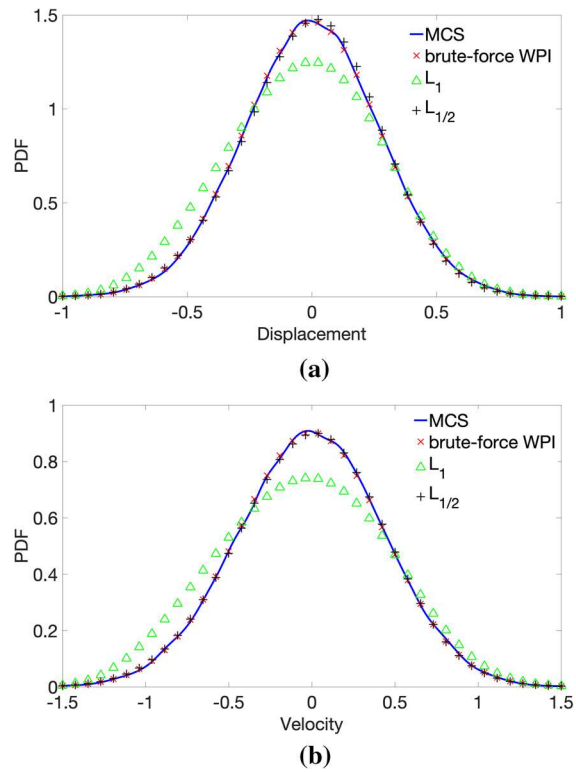

Fig. 6 Marginal PDF of an oscillator with asymmetric nonlinearities at $t = 1s$: **a** displacement and **b** velocity; comparisons between $L_{1/2}$-norm, L_1-norm approaches for $r/n_j = 0.3$ and MCS data (10,000 realizations). Results based on a brute-force implementation of the WPI technique are included as well

and

$$h(x) = \begin{cases} (x-a)^{3/2} & \text{if } x \geq a \\ 0 & \text{otherwise} \end{cases} \tag{30}$$

In Eqs. (29)–(30), η denotes a parameter accounting for the nonlinearity degree, and a represents the displacement bound. The interested reader is also directed to the review paper [33] for more details and for a broader perspective. Further, the exact stationary joint response PDF takes the form [33]

$$p(x,\dot{x}) = \begin{cases} Ce^{-\frac{x^2}{2\sigma_0^2}-\frac{\dot{x}^2}{2\sigma_0^2\omega_0^2}-\zeta\frac{(x-a)^{5/2}}{\sigma_0^{5/2}}} & \text{if } x \geq a \\ Ce^{-\frac{x^2}{2\sigma_0^2}-\frac{\dot{x}^2}{2\sigma_0^2\omega_0^2}} & \text{if } x < a \end{cases} \tag{31}$$

where

$$k = \omega_0^2; \quad \zeta = \frac{2\eta\sqrt{\sigma_0}}{5\omega_0^2}; \quad \sigma_0^2 = \frac{\pi S_0}{2c\omega_0^2} \tag{32}$$

and C is a normalization constant.

It can be readily seen that due to the form of the nonlinear function and specifically due to the presence of the non-integer power in the expression of Eq. (30), a standard polynomial expansion cannot model the response PDF exactly. This is obvious in Eq. (31) where the stationary response PDF comprises a term of power 5/2. Moreover, depending on the magnitude of the nonlinearity controlled by parameter η, the joint response PDF shape can experience abrupt changes (in the region around the displacement bound) that may require higher-order polynomial expansions for their accurate representation. Clearly, not only a PDF expansion based on a standard polynomial basis is not sparse,

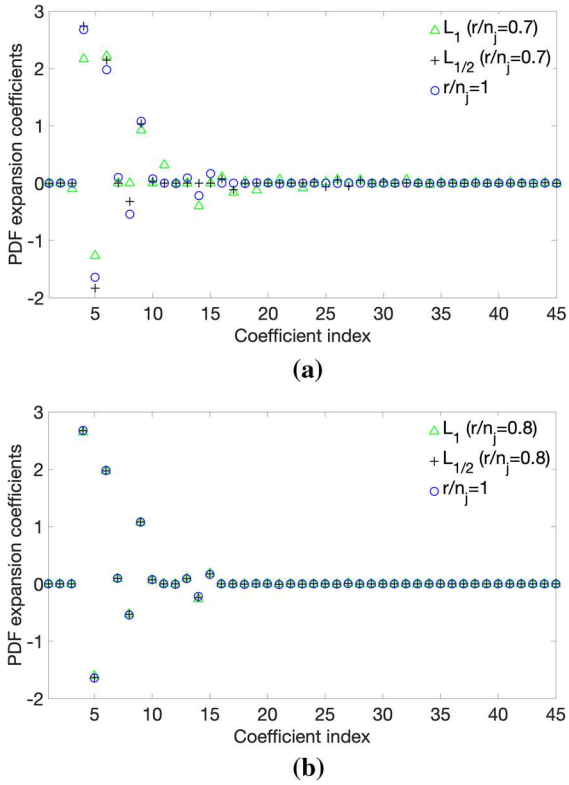

Fig. 7 Joint response PDF polynomial expansion coefficients corresponding to an oscillator with asymmetric nonlinearities at $t = 2s$ with **a** $r/n_j = 0.7$ and **b** $r/n_j = 0.8$

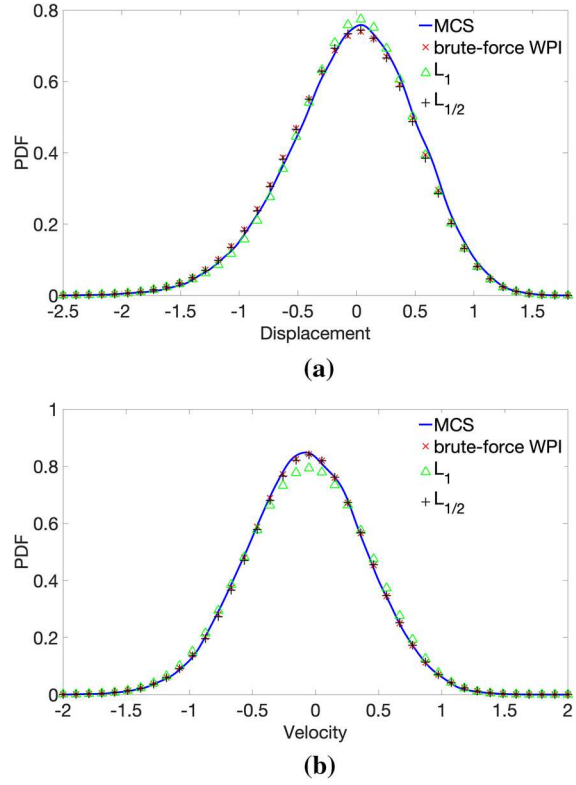

Fig. 8 Marginal PDF of an oscillator with asymmetric nonlinearities at $t = 2s$: **a** displacement and **b** velocity; comparisons between $L_{1/2}$-norm, L_1-norm approaches for $r/n_j = 0.7$ and MCS data (10,000 realizations). Results based on a brute-force implementation of the WPI technique are included as well

but also the monomial basis is prone to ill-conditioning as noted in [14]. In fact, attempting to use the same basis for the spatial domain as in examples 3.1 and 3.2, employing both 8th- and 12th-order polynomial expansions, has led to ill-conditioning of the resulting interpolation matrix. Therefore, to bypass this limitation, a Kronecker expansion in the form of Eq. (12) utilizing harmonic wavelets both in the space and the time domains is used next with $N_{s1} = N_{s2} = 20$ and $N_t = 16$, and parameter values $S_0 = 1.0192, k = 0.3, c = 0.5, \eta = 5, a = 0.5$.

Figure 9 shows the computed harmonic wavelet expansion coefficients corresponding to $t = 1.2s$, using both $r/n_j = 0.3$ and $r/n_j = 0.4$. Compared to the solution based on $r/n_j = 1$, it is seen that both the $L_{1/2}$-norm and the L_1-norm approaches exhibit high accuracy in recovering the sparse coefficient vector for $r/n_j = 0.4$. However, the $L_{1/2}$-norm approach appears to yield a sparser (and more accurate) solution when fewer PDF measurements are used, i.e., for $r/n_j = 0.3$.

In Fig. 10, the corresponding PDF estimates are plotted and compared with pertinent MCS results (10,000 realizations). It is seen that $L_{1/2}$-norm minimization yields a solution that exhibits better agreement with MCS data than the one obtained by L_1-norm minimization. Results based on a brute-force implementation of the WPI technique relying on a discretization of the PDF effective domain are included as well.

Next, attention is directed to $t = 6.4s$ corresponding to the stationary phase of the response process. Similarly to the $t = 1.2s$ case, the estimated coefficient vector based on $L_{1/2}$-norm exhibits better agreement with the solution based on $r/n_j = 1$ than the estimate based on L_1-norm. This is shown in Fig. 11, where both $r/n_j = 0.3$ and $r/n_j = 0.4$ are used. Further, the PDF estimates based on L_1-norm and $L_{1/2}$-norm are plotted in Fig. 12 and compared with the exact response PDF of Eq. (31). It is seen that even for this highly asymmetric response displacement PDF featuring an abrupt

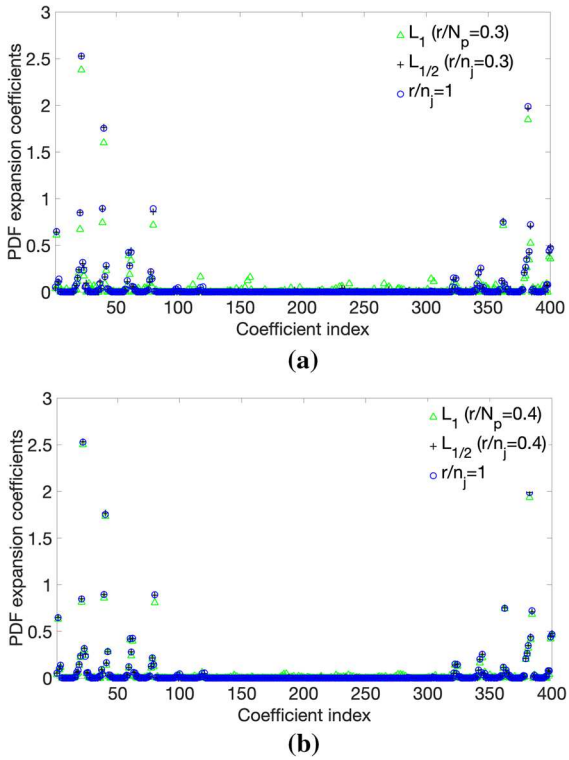

Fig. 9 Joint response PDF harmonic wavelet expansion coefficients corresponding to a nonlinear vibro-impact oscillator at $t = 1.2s$ with **a** $r/n_j = 0.3$ and **b** $r/n_j = 0.4$

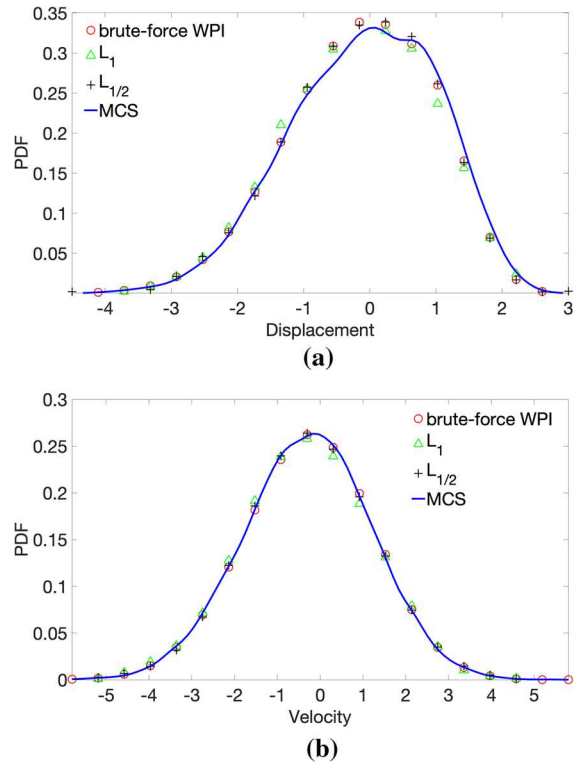

Fig. 10 Nonlinear vibro-impact oscillator marginal response PDF at $t = 1.2s$: **a** displacement and **b** velocity; comparisons between $L_{1/2}$-norm and L_1-norm approaches for $r/n_j = 0.3$ and MCS data (10,000 realizations). Results based on a brute-force implementation of the WPI technique are included as well

change in its shape, $L_{1/2}$-norm minimization provides a solution of satisfactory accuracy requiring only few PDF measurements. Also, it consistently outperforms L_1-norm minimization in terms of achieved accuracy. More specifically, referring to the exact joint response PDF of Eq. (31), the root-mean-square errors corresponding to the estimates obtained based on L_1- and $L_{1/2}$-norms are equal to 5% and 1%, respectively.

4 Concluding remarks

In this paper, the WPI technique for determining the stochastic response of diverse nonlinear dynamical systems has been extended and its computational efficiency has been enhanced by relying on sparse representations and compressive sampling concepts and tools. Specifically, relying on the localization capabilities of the WPI technique for evaluating directly specific points of the joint response PDF, and utilizing appropriately selected bases for expanding the PDF, has led to an underdetermined system of equations for the expansion coefficient vector. This has been solved by employing an $L_{1/2}$-norm minimization formulation. Notably, the proposed $L_{1/2}$-norm formulation has exhibited an enhanced sparsity-promoting behavior compared to an alternative standard L_1-norm minimization approach. In other words, the sparse PDF expansion coefficient vector can be determined by utilizing fewer PDF points, thus leading to a significant reduction of the associated computational cost since fewer BVPs need to be solved numerically. Moreover, it has been shown that utilizing the same number of PDF points obtained by the WPI, $L_{1/2}$-norm minimization yields more accurate PDF estimates than an L_1-norm approach. Comparisons with pertinent MCS data have demonstrated the reliability of the developed technique. This has been done in conjunction with various stochastically excited oscillators exhibiting diverse nonlinear behaviors, including a Duffing oscillator, an oscillator

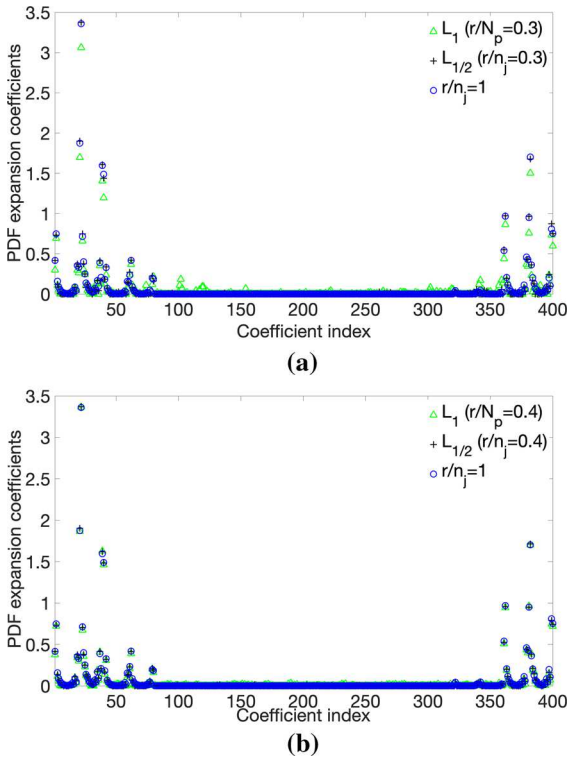

Fig. 11 Joint response PDF harmonic wavelet expansion coefficients corresponding to a nonlinear vibro-impact oscillator at $t = 6.4s$ (stationary phase) with **a** $r/n_j = 0.3$ and **b** $r/n_j = 0.4$

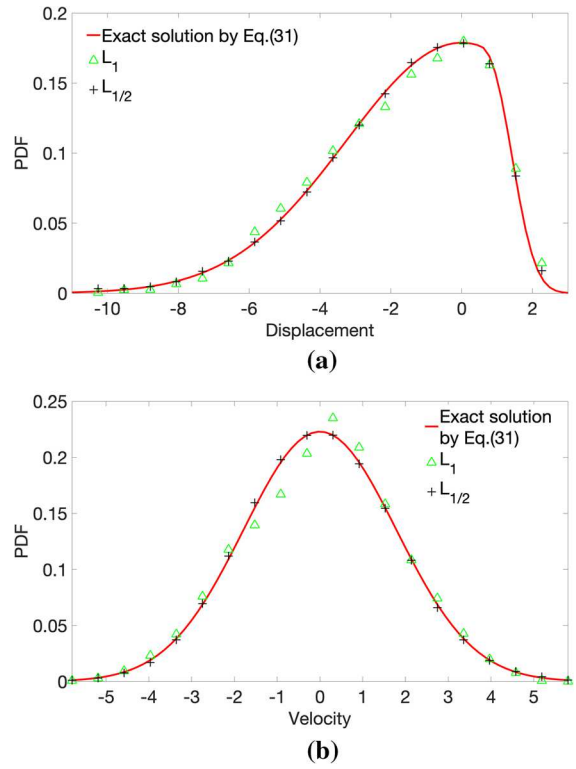

Fig. 12 Vibro-impact oscillator marginal response PDF at $t = 6.4s$ (stationary phase): **a** displacement and **b** velocity; comparisons between $L_{1/2}$-norm and L_1-norm approaches for $r/n_j = 0.3$ and the exact solution of Eq. (31)

with asymmetric nonlinearities, and a nonlinear vibro-impact oscillator.

Acknowledgements I. A. Kougioumtzoglou gratefully acknowledges the support through his CAREER award by the CMMI Division of the National Science Foundation, USA (Award no. 1748537). Y. Zhang acknowledges the support by "the Fundamental Research Funds for the Central Universities (WUT:2021IVA091)". F. Kong acknowledges the support by the National Natural Science Foundation of China (Grant no. 52078399).

Data availability The datasets generated during and/or analyzed during the current study are available from the corresponding author on reasonable request.

Declarations

Conflict of interest The authors declare that they have no conflict of interest.

Appendix

In this Appendix, more details are provided on the derivation of the Euler–Lagrange Eq. (5) to be solved in conjunction with the boundary conditions of Eq. (6) for determining the WPI most probable path (see also Refs. [11,12]). Specifically, considering the Lagrangian functional of Eq. (3), the stochastic action $S[x, \dot{x}, \ddot{x}]$ is defined as

$$S[x, \dot{x}, \ddot{x}] = \int_{t_i}^{t_f} L[x, \dot{x}, \ddot{x}]dt \tag{A.1}$$

Next, by utilizing a functional Taylor-type series expansion of the stochastic action $S[x, \dot{x}, \ddot{x}]$ and by expressing $x(t)$ as

$$x(t) = x_c(t) + X(t) \tag{A.2}$$

the stochastic action S is written as:

$$S[x] = S[x_c + X] = S[x_c] + \delta S[x_c, X] + \frac{1}{2!}\delta^2 S[x_c, X] + \ldots \tag{A.3}$$

In Eq. (A.3), $x_c(t)$ is the path associated with the maximum probability of occurrence and $X(t)$, with $X(t_i) = X(t_f) = \dot{X}(t_i) = \dot{X}(t_f) = 0$, represents the fluctuations around $x_c(t)$ (e.g., [8]). In Eq. (A.3), $S[x, \dot{x}, \ddot{x}]$ is denoted as $S[x]$ for simplicity, and $\delta S[x_c, X]$ represents the functional differential (or variation) of S evaluated on x_c. Moreover, according to calculus of variations [17] and considering Eqs. (A.1) and (A.3), the differential $\delta S[x_c, X]$ takes the form

$$\delta S[x_c, X] = \int_{t_i}^{t_f} \left(\left.\frac{\partial L}{\partial x}\right|_{x=x_c} X + \left.\frac{\partial L}{\partial \dot{x}}\right|_{x=x_c} \dot{X} + \left.\frac{\partial L}{\partial \ddot{x}}\right|_{x=x_c} \ddot{X} \right) dt \tag{A.4}$$

Further, considering Eqs. (2) and (A.1), it is seen that the maximum probability of occurrence corresponds to minimum $S[x, \dot{x}, \ddot{x}]$. Thus, $x_c(t)$ is associated with an extremum of the functional $S[x, \dot{x}, \ddot{x}]$. In this context, calculus of variations dictates [17] that the first variation of $S[x, \dot{x}, \ddot{x}]$ vanishes for $x(t) = x_c(t)$, i.e.,

$$\delta S[x_c, X] = 0 \tag{A.5}$$

Therefore, Eq. (A.3) becomes

$$S[x] = S[x_c] + \frac{1}{2!}\delta^2 S[x_c, X] + \ldots \tag{A.6}$$

Furthermore, combining Eq. (A.4) and the extremality condition of Eq. (A.5) yields

$$\int_{t_i}^{t_f} \left(\left.\frac{\partial L}{\partial x}\right|_{x=x_c} X + \left.\frac{\partial L}{\partial \dot{x}}\right|_{x=x_c} \frac{d}{dt} X + \left.\frac{\partial L}{\partial \ddot{x}}\right|_{x=x_c} \frac{d^2}{dt^2} X \right) dt = 0 \tag{A.7}$$

Next, integrating Eq. (A.7) by parts leads to

$$\underbrace{\left[\left(\left.\frac{\partial L}{\partial \dot{x}}\right|_{x=x_c} - \frac{d}{dt}\left.\frac{\partial L}{\partial \ddot{x}}\right|_{x=x_c} \right) X(t) \right]_{t_i}^{t_f}}_{\mathscr{A}_0} + \underbrace{\left[\left.\frac{\partial L}{\partial \ddot{x}}\right|_{x=x_c} \dot{X}(t) \right]_{t_i}^{t_f}}_{\mathscr{A}_1} + \underbrace{\int_{t_i}^{t_f} \left(\left.\frac{\partial L}{\partial x}\right|_{x=x_c} - \frac{d}{dt}\left.\frac{\partial L}{\partial \dot{x}}\right|_{x=x_c} + \frac{d^2}{dt^2}\left.\frac{\partial L}{\partial \ddot{x}}\right|_{x=x_c} \right) X(t) dt}_{\mathscr{B}} = 0 \tag{A.8}$$

where, since $X(t_i) = X(t_f) = \dot{X}(t_i) = \dot{X}(t_f) = 0$, the terms $\mathscr{A}_0$ and $\mathscr{A}_1$ vanish. Thus, Eq. (A.8) yields the Euler–Lagrange Eq. (5) to be solved in conjunction with the boundary conditions of Eq. (6) for determining the WPI most probable path x_c.

Note that x_c can be used, at least in principle, for evaluating the higher-order terms in the expansion of Eq. (A.6). However, in the majority of practical implementations of the WPI technique, only the first term $S[x_c]$ is retained in the expansion of Eq. (A.6), since the evaluation of higher-order terms exhibits considerable analytical and computational challenges. In fact, in the most probable path approximation shown in Eq. (7) the remaining terms in the expansion of Eq. (A.6) are treated collectively as a constant C. The interested reader is also directed to [12], where a quadratic approximation was developed for the WPI that accounts explicitly for the contribution also of the second variation term in Eq. (A.6).

References

1. Eom, K., Park, H.S., Yoon, D.S., Kwon, T.: Nanomechanical resonators and their applications in biological/chemical detection: Nanomechanics principles. Phys. Rep. **503**(4–5), 115–163 (2011)
2. Daqaq, M.F., Masana, R., Erturk, A., Dane Quinn, D.: On the role of nonlinearities in vibratory energy harvesting: a critical review and discussion. Appl. Mech. Rev. **66**(4), (2014)
3. Roberts, J.B., Spanos, P.D.: Random Vibration and Statistical Linearization. Dover, New York (2003)
4. Li, J., Chen, J.: Stochastic Dynamics of Structures. Wiley, New York (2009)
5. Grigoriu, M.: Stochastic Systems: Uncertainty Quantification and Propagation. Springer, Berlin (2012)
6. Daniell, P.J.: Integrals in an infinite number of dimensions. Ann. Math. pp 281–288, (1919)
7. Wiener, N.: The average of an analytic functional. Proc. Natl. Acad. Sci. U. S. America **7**(9), 253 (1921)

8. Chaichian, M., Demichev, A.: Path Integrals in Physics: Volume I Stochastic Processes and Quantum Mechanics. CRC Press, Boca Raton (2001)
9. Kougioumtzoglou, I., Spanos, P.: An analytical Wiener path integral technique for non-stationary response determination of nonlinear oscillators. Probab. Eng. Mech. **28**, 125–131 (2012)
10. Petromichelakis, I., Psaros, A.F., Kougioumtzoglou, I.A.: Stochastic response determination of nonlinear structural systems with singular diffusion matrices: A Wiener path integral variational formulation with constraints. Probab. Eng. Mech. **60**, 103044 (2020)
11. Psaros, A.F., Brudastova, O., Malara, G., Kougioumtzoglou, I.A.: Wiener path integral based response determination of nonlinear systems subject to non-white, non-Gaussian, and non-stationary stochastic excitation. J. Sound Vib. **433**, 314–333 (2018)
12. Psaros, A.F., Kougioumtzoglou, I.A.: Functional series expansions and quadratic approximations for enhancing the accuracy of the Wiener path integral technique. J. Eng. Mech. **146**(7), 04020065 (2020)
13. Petromichelakis, I., Kougioumtzoglou, I.A.: Addressing the curse of dimensionality in stochastic dynamics: a Wiener path integral variational formulation with free boundaries. Proc. R. Soc. A **476**, 20200385 (2020)
14. Psaros, A.F., Kougioumtzoglou, I.A., Petromichelakis, I.: Sparse representations and compressive sampling for enhancing the computational efficiency of the Wiener path integral technique. Mech. Syst. Signal Process. **111**, 87–101 (2018)
15. Psaros, A.F., Petromichelakis, I., Kougioumtzoglou, I.A.: Wiener path integrals and multi-dimensional global bases for non-stationary stochastic response determination of structural systems. Mech. Syst. Signal Process. **128**, 551–571 (2019)
16. Kougioumtzoglou, I.A., Petromichelakis, I., Psaros, A.F.: Sparse representations and compressive sampling approaches in engineering mechanics: A review of theoretical concepts and diverse applications. Probab. Eng. Mech. **61**, 103082 (2020)
17. Ewing, G.M.: Calculus of Variations with Applications. Dover Publications, Mineola (1985)
18. Psaros, A.F., Zhao, Y., Kougioumtzoglou, I.A.: An exact closed-form solution for linear multi-degree-of-freedom systems under Gaussian white noise via the Wiener path integral technique. Probab. Eng. Mech. **60**, 103040 (2020)
19. Kougioumtzoglou, IA., Di Matteo, A., Spanos, PD., Pirrotta, A., Di Paola, M.: An efficient Wiener path integral technique formulation for stochastic response determination of nonlinear mdof systems. J. Appl. Mech. **82**(10):101005: 1–7, (2015)
20. Rish, I., Grabarnik, G.: Sparse Modeling: Theory, Algorithms, and Applications. CRC Press, Boca RatonBoca Raton (2014)
21. Foucart, S., Rauhut, H.: A mathematical introduction to compressive sensing. Bull. Am. Math. **54**(2017), 151–165 (2017)
22. Olver, P.J.: On multivariate interpolation. Stud. Appl. Math. **116**(2), 201–240 (2006)
23. Mallat, S.: A Wavelet Tour of Signal Processing. Elsevier, Amsterdam (1999)
24. Fasshauer, G.E.: Positive definite kernels: past, present and future. Dolomites Res. Notes Approx. **4**, 21–63 (2011)
25. Caiafa, C.F., Cichocki, A.: Computing sparse representations of multidimensional signals using kronecker bases. Neural Comput. **25**(1), 186–220 (2013)
26. Newland, D.E.: Harmonic and musical wavelets. Proc. R. Soc. Lond. Ser. A Math. Phys. Sci. **444**(1922), 605–620 (1994)
27. Zhang, Y., Comerford, L., Kougioumtzoglou, I.A., Beer, M.: Lp-norm minimization for stochastic process power spectrum estimation subject to incomplete data. Mech. Syst. Signal Process. **101**, 361–376 (2018)
28. Xu, Z., Zhang, H., Wang, Y., Chang, X., Liang, Y.: L 1/2 regularization. Sci. China Inf. Sci. **53**(6), 1159–1169 (2010)
29. Gorodnitsky, I.F., Rao, B.D.: Sparse signal reconstruction from limited data using focuss: A re-weighted minimum norm algorithm. IEEE Trans. Signal Process. **45**(3), 600–616 (1997)
30. Chartrand, R., Yin, W.: Iteratively reweighted algorithms for compressive sensing. In: 2008 IEEE international conference on acoustics, speech and signal processing, IEEE, pp 3869–3872, (2008)
31. Van Barel, M., Humet, M., Sorber, L.: Approximating optimal point configurations for multivariate polynomial interpolation. Electron. Trans. Numer. Anal. **42**, 41–63 (2014)
32. Lin, Y.K.: Probabilistic Theory of Structural Dynamics. McGraw-Hill, New York (1967)
33. Dimentberg, M., Iourtchenko, D.: Random vibrations with impacts: a review. Nonlinear Dyn. **36**(2), 229–254 (2004)